ACS APPLIED MATERIALS & INTERFACES

Research Article

www.acsami.org

Mechanistic Insight into the Chemical Exfoliation and Functionalization of Ti_3C_2 MXene

Pooja Srivastava,[†,‡] Avanish Mishra,[†,‡] Hiroshi Mizuseki,[§] Kwang-Ryeol Lee,[§] and Abhishek K. Singh*[,†]

[†]Materials Research Centre, Indian Institute of Science, Bangalore 560012, India

[§]Computational Science Research Center, Korea Institute of Science and Technology (KIST), Seoul 02792, Republic of Korea

Supporting Information

ABSTRACT: MXene, a two-dimensional layer of transition metal carbides/nitrides, showed great promise for energy storage, sensing, and electronic applications. MXene are chemically exfoliated from the bulk MAX phase; however, mechanistic understanding of exfoliation and subsequent functionalization of these technologically important materials is still lacking. Here, using density-functional theory we show that exfoliation of Ti_3C_2 MXene proceeds via HF insertion through edges of Ti_3AlC_2 MAX phase. Spontaneous dissociation of HF and subsequent termination of edge Ti atoms by H/F weakens Al−MXene bonds. Consequent opening of the interlayer gap allows further insertion of HF that leads to the formation of AlF_3 and H_2, which eventually come out of the MAX, leaving fluorinated MXene behind. Density of state and electron localization function shows robust binding between F/OH and Ti, which makes it very difficult to obtain controlled functionalized or pristine MXene. Analysis of the calculated Gibbs free energy (ΔG) shows fully fluorinated MXene to be lowest in energy, whereas the formation of pristine MXene is thermodynamically least favorable. In the presence of water, mixed functionalized $Ti_3C_2F_x(OH)_{1-x}$ (x ranges from 0 to 1) MXene can be obtained. The ΔG values for the mixed functionalized MXenes are very close in energy, indicating the random and nonuniform functionalization of MXene. The microscopic understanding gained here unveils the challenges in exfoliation and controlling the functionalization of MXene, which is essential for its practical application.

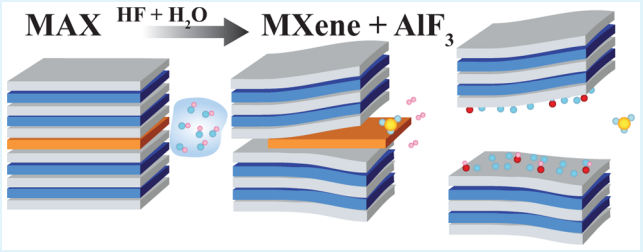

KEYWORDS: *MXene, Ti_3AlC_2, functionalization, thermodynamics, Gibbs free energy of reaction*

INTRODUCTION

Two-dimensional (2D) layers of early transition metal carbides or/and nitrides,[1,2] called MXene, have stimulated research enthusiasm due to their unusual combination of metallic conductivity and excellent structural and chemical stabilities of ceramics. Ti_3C_2, owing to its technological importance, is the most extensively studied MXene. Its potential as electrode for energy storage applications, such as Li/Na ion batteries, supercapacitors and fuel cells,[3−10] antibacterial film,[11] charge- and size-selective ion sieving membrane,[11] and transparent conductors in electronic, electrochromic, and sensor applications,[12−14] has already been demonstrated in laboratories. Ti_3C_2 is exfoliated from the Ti_3AlC_2 using HF, and its surface is randomly and nonuniformly covered by various F- and O-containing functional groups.[15] To emphasize the presence of the functional group, Ti_3C_2 is often presented as $Ti_3C_2T_x$, where T = F, OH, and O. In order to scale up these applications to the industrial level, the challenges associated with the isolation of high-quality pristine or uniformly functionalized MXene need to be addressed.

Assuming full coverage of functional groups on Ti_3C_2 various appealing predictions are made by theoretical studies such as ionic sieving through $Ti_3C_2(OH)_2$,[16] semiconducting gap in $Ti_3C_2(F)_2$,[1] and ultralow work function of $Ti_3C_2(OH)_2$.[17] On the other hand, Tang et al. predicted that the Li storage capacity of functionalized Ti_3C_2 is inferior to that of pristine Ti_3C_2.[18] The presence of functional groups on MXene also deteriorates the hydrogen storage capacity of Ti_3C_2.[9] Furthermore, both the absorptions and the reflectivity of Ti_3C_2 crucially depend upon the presence and type of functional group on the surface.[12,13] This work emphasizes the importance of pristine as well as controlled functionalized MXene. Unlike graphene or other 2D materials, the functional groups terminations in MXene are not due to any controlled reaction but the result of the exfoliation process itself, therefore further necessitating an in-depth understanding of the exfoliation and simultaneous functionalization process.

For other 2D materials, like graphene,[19−23] MoS_2,[24] and phosphorene,[25] where the weak van der Waals interaction holds the layers together, the exfoliation process is extensively studied and well understood. However, in MAX phase the interleaved Al atoms bind the MXene layers via strong metallic Ti−Al[3,26−29] bonds. Therefore, the exfoliation process of MXene is inherently more complicated and different from that of van der

Received: July 10, 2016
Accepted: August 18, 2016
Published: August 18, 2016

DOI: 10.1021/acsami.6b08413
ACS Appl. Mater. Interfaces 2016, 8, 24256−24264

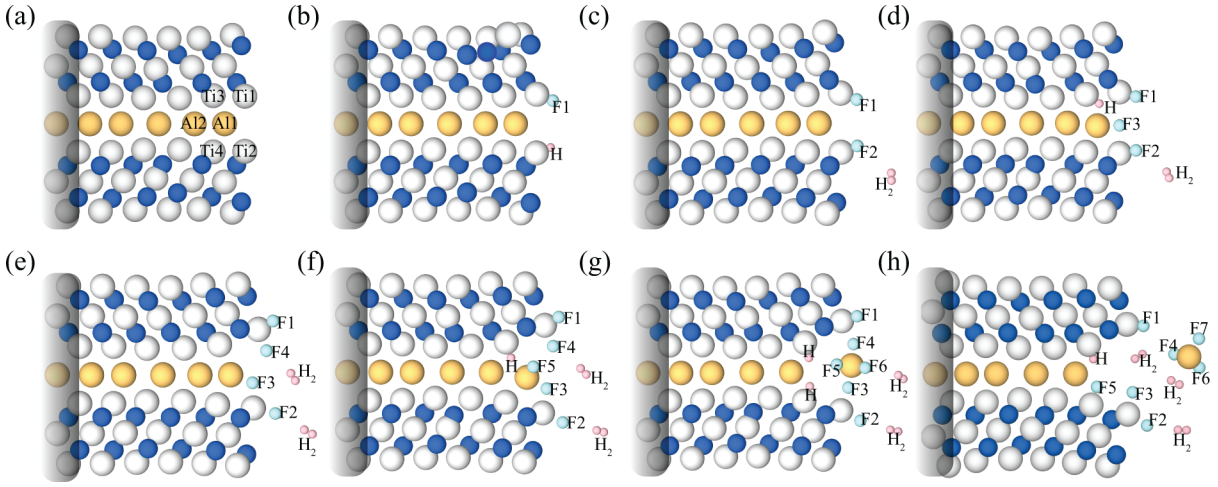

Figure 1. Lowest energy atomic configurations during the step-by-step intercalation of HF via the Ti_3AlC_2 edge and extraction of AlF_3: (a) pristine and (b) one, (c) two, (d) three, (e) four, (f) five, (g) six, and (h) seven HF-intercalated MAX complexes. Atoms at left edge are fixed and shown here by shaded region. Silver, blue, orange, cyan, and pink balls represent Ti, C, Al, F, and H atoms, respectively.

Waals solids. However, to date no attempt has been made to develop a comprehensive understanding of the reaction between MAX phase and HF, which facilitates the exfoliation and subsequent functionalization of MXene. Using density-functional theory (DFT), we report the detailed mechanism of the exfoliation and functionalization of Ti_3C_2 due to the intercalation of HF via the edges of Ti_3AlC_2. The spontaneous dissociation of HF leads to the termination of edge Ti atoms of the two layers and initiates the exfoliation process. The H/F terminations essentially increase the interlayer spacing and facilitate further inclusion of HF, which eventually leads to the formation of AlF_3 and H_2. The AlF_3 and H_2 come out of the system, leaving F-functionalized MXene behind. In the entire range of chemical potentials of hydrogen, the Gibbs free energy (ΔG) of the uniformly F-functionalized MXene is lowest, whereas that for pristine MXene is highest. In the presence of H_2O, ΔG of all reactions involving full and mixed functionalization with varying concentrations of F and OH are very close in energy and therefore almost equally probable. This will lead to random and nonuniform functionalization of MXene. The density of states and electron-localized function reveal robust bonding between F/OH and Ti, which highlights the challenges associated with the isolation of uniformly functionalized or pristine MXene. Furthermore, at high concentrations of HF/H_2O, the formation of $TiF_4/TiF_3/TiO_2$ and graphite becomes thermodynamically favorable, indicating the possibility of degradation of MXene under very high concentrations of HF or moist environment.

METHODOLOGY

All calculations were performed within the framework of density-functional theory (DFT) using the Vienna ab initio Simulation Package (VASP).[30] The wave functions are expressed in a plane wave basis set with an energy cutoff of 500 eV. Electron−ion interactions and electronic exchange correlations are treated with all-electron projector augmented wave potentials (PAW).[31] The exchange-correlation energy is represented by a gradient-corrected (GGA)[31,32] functional proposed by Perdew, Burke, and Ernzerhof (PBE).[33] Brillouin zone integrations are performed using a 4 × 1 × 1 Monkhorst−Pack[34] k-point mesh. The positions of all atoms are relaxed using the conjugate-gradient method until the component of force on each atom is less than $\leq 10^{-3}$ eV/Å. For density of state calculation the Brillouin zone has been sampled using a 15 × 1 × 1 k-grid. In all structures, the vacuum region between two adjacent periodic images are fixed to 20 Å to avoid spurious interaction among periodic images. Ab-initio molecular dynamics (AIMD) simulation were performed to access the effects of HF concentration and temperature on the exfoliation process with a time step of 1 fs within the canonical ensemble. The temperature was set at 300 K and adjusted via a Nosé−Hover thermostat.[35−37] For AIMD calculations, the plane wave basis set cutoff is set at 350 eV.

RESULTS AND DISCUSSION

To gain a comprehensive understanding of the exfoliation of MXene, we constructed a model structure for the MAX phase, as shown in Figure S1 in the Supporting Information. The MAX phase is modeled as bilayer Ti_3C_2 MXene with a layer of Al atoms interleaved between them. Al atom occupies a position on Ti (mid sublayer) top site and bonded with 6 nearby Ti atoms (Figure S1 in the Supporting Information). We considered a 6 × 1 × 1 MAX supercell with 20 Å vacuum in the Y and Z direction for the intercalation of HF via the MAX edges as shown in Figure 1a. Atoms at the left most edge of the MAX (Figure 1b−h) are fixed, and all other atoms are fully relaxed. Exfoliation of graphene[38,39] or phosphorene[25] also involves the penetration of solvent moieties via the sample edges, which opens interlayer gaps. In these van der Waals solids, the binding forces between the layers vary as r^{-6}, where r is the interlayer distance.[40] Intercalating species disrupt bonding between the layers by increasing the interlayer distance leading to isolation of layers. However, in MAX, a strong chemical binding between the MXene layers via Al makes the exfoliation process very complex and challenging.[41] In order to simulate this, we add HF molecules one by one at the open edge of MAX phase, followed by complete structural relaxation. Various configurations of HF-MAX complex are considered, and the minimum energy structure was taken for inclusion of the next HF molecule. The evolution of the lowest energy atomic configuration during the intercalation of 1−7 HF molecules is shown in Figure 1b−h.

The intercalation starts with the spontaneous dissociation of HF and subsequent termination of undercoordinated Ti atoms at the edge by both H and F atoms (Figure 1b). Due to H and F terminations the Al1−Ti1 and Al1−Ti2 bond lengths increases slightly (~2% and 0.6%) (Figure 1b). Second HF insertion also results in the spontaneous termination of both

DOI: 10.1021/acsami.6b08413
ACS Appl. Mater. Interfaces 2016, 8, 24256−24264

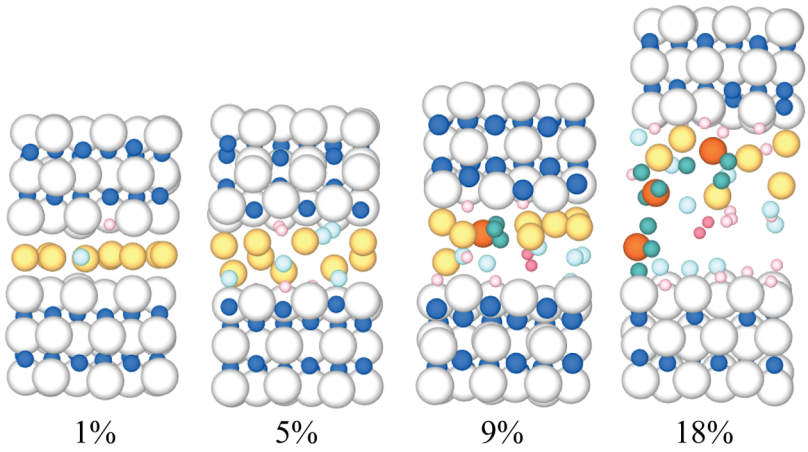

Figure 2. AIMD snapshots of the HF−Ti_3AlC_2 at different concentrations of HF 1%, 5%, 9%, and 18% at t = 30 ps. Silver, blue, orange, cyan, and pink balls represent Ti, C, Al, F, and H atoms, respectively. To highlight the formation of AlF_3 and H_2, darker shades are used to present Al, F, and H atoms.

Ti1 and Ti2 atoms at the edge by F atoms and results in the weakening of both edge Al1−Ti bonds as evident from the increase in Al1−Ti1 and Al1−Ti2 bond length (Figure 1c). Interestingly, H_2 molecule (Figure 1c) forms, when two H atoms are available there. The third HF molecule also dissociated into H and F, with H binding to the Ti3 atom and F binding with the Al1 atom at the edge (Figure 1d). Al1−Ti1 bond length increases up to ∼14% of its original length. Addition of a fourth HF leads to the F termination of already F-terminated Ti1 and formation of two H_2 molecules. Due to the repulsion from F4, F3 moves toward the Ti2 and forms a weak bond with it as shown in Figure 1e. The length of Al1−Ti1 and Al1−Ti2 bonds increases by ∼47% and 11%, respectively, indicating the dissociation/weakening of Al1−Ti1 and Al1−Ti2 bonds. Addition of a fifth HF results in the H termination of the Ti3 atom and F termination of Al1 as shown in Figure 1f, which severely weakens bonding of Ti3 with Al1. A sixth HF insertion results in termination of Ti3 and Ti4 atoms by H atoms. Bonding of F6 with Al1 leads to the formation of two strong Al1−F bonds. As Al1 is also weakly bonded with the Ti1 and Ti2 atoms, this AlF_4 is a precursor of AlF_3 (Figure 1g). The bond length of Al1−F5 is ∼2% larger than the other Al1−F bond and can be identified as the weakest among all the Al1−F bonds. Addition of a seventh HF leads to dissociation of the Al1−F5 bond and formation of a Al1−F7 bond. The binding of F5 with Ti3 and dissociation of F4−Ti1 bonds result in the formation of AlF_3, which eventually leaves F/H-terminated MXene layer (Figure 1h) behind. Experimental studies have confirmed the formation of AlF_3 during the isolation of MXene from MAX.[1] The analysis presented here, clearly reveals that F (or H) termination of MXene is essential for the weakening of Al−MXene bonds, which subsequently facilitate the formation of AlF_3. However, requirement of seven HF molecules for extraction of first AlF_3 imposes significant constrains over the exfoliation process. Furthermore, H atoms provide active support by forming H−Ti intermediates, which eventually forms H_2 molecule in the presence of another H atom. This H_2 evolution[1,42] during the reaction has also been supported by the experiments.

Effect of H_2O. In practical experimental conditions, the aqueous solution of HF is usually employed for the exfoliation of MXene from MAX. Therefore, during the reaction the intercalation of H_2O molecules into the MAX is plausible. A perusal of MXene literature also shows the presence of a −OH functional group on the MXene surface, which indicates the active role played by the water molecules in the isolation process. To understand the role of water in the isolation of MXene, we intercalated one H_2O molecule at the MAX edge. The spontaneous dissociation of H_2O into −H and −OH followed by termination of edge Ti atoms by H/OH functional group is observed (Figure S2 in the Supporting Information). The formation energy (E^f, as discussed in Supporting Information) of H_2O-intercalated MAX is ∼0.2 eV more than that of HF-intercalated MAX, thus indicating the preference for the HF over H_2O intercalation. We further compared the E^f of MAX with (i) two HF, (ii) two H_2O, and (iii) one HF and one H_2O molecules. We find that the E^f is minimum when two F atoms terminate the edge Ti atoms. The E^f of structure with one F and one OH terminating the edge Ti atoms was higher by 0.21 eV, whereas the formation of OH-terminated MAX was energetically least favorable (by 0.65 eV compared to two F case). These observations clearly show the preference for F terminations. Experimentally, it has been shown that under ambient conditions the formation of AlF_3 is preferred over $Al(OH)_3$.[43] Therefore, it indicates that the termination of Al/Ti atoms by HF initiates and carries out the MXene isolation process, and H_2O supports the exfoliation process by delaminating the MXene layers. It also explains the experimental finding of functionalized MXene primarily by F atoms.[15]

Exfoliation Process with Varying Concentrations of HF. Generally, the rate of reaction crucially depends on the concentration of reactants and temperature. To understand the effects of concentration on the isolation process we performed ab initio molecular dynamics (AIMD) simulations for the MAX and HF system. Usually the exfoliation of MXene occurs at room temperature; therefore, the temperature is set at 300 K. AIMD simulation is performed for various concentrations of HF-1%, -5%, -9%, and -18%. AIMD is a powerful tool to assess the dynamics of the real systems at finite temperature; here the forces are calculated on-the-fly from accurate electronic structure calculations. We employed the relaxed geometry of the HF-intercalated MXene and observed the dynamics up to 30 ps. The snapshots of AIMD simulation at 30 ps for all the concentration of HF considered here, are shown in Figure 2. At low concentration of HF, the F atom binds with Al.

DOI: 10.1021/acsami.6b08413
ACS Appl. Mater. Interfaces 2016, 8, 24256−24264

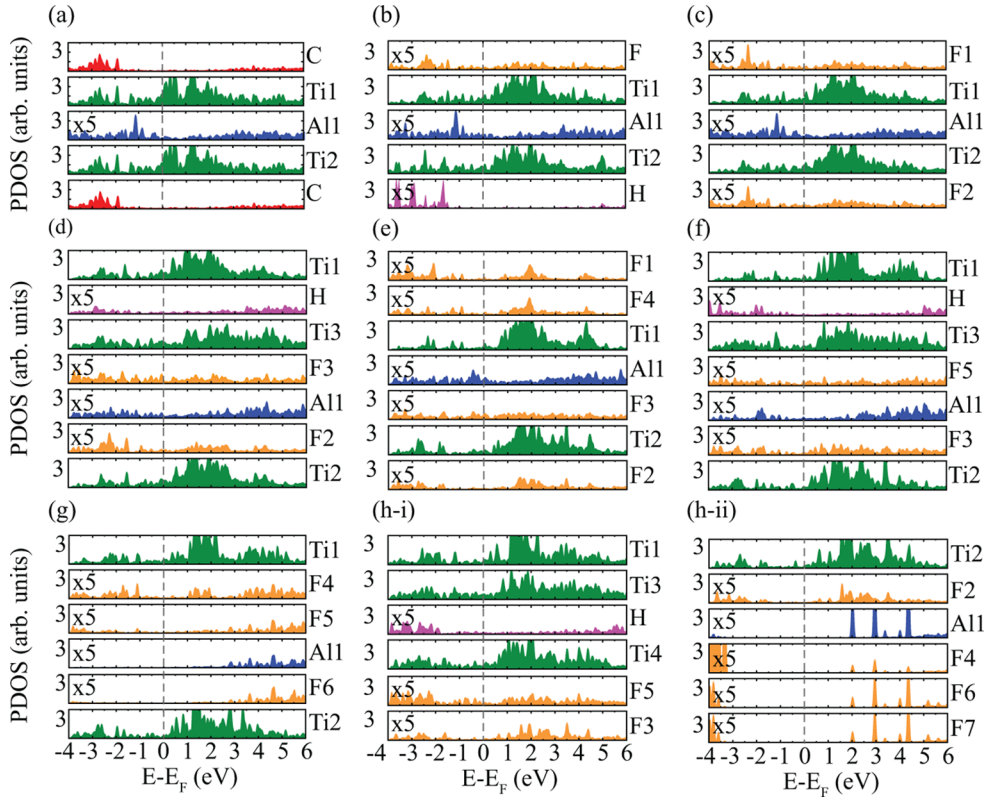

Figure 3. *l*-projected PDOS for (a) pristine and (b–h) 1–7 HF-intercalated Ti_3AlC_2. For clarity, h is presented in two parts (i and ii). Fermi level is set at zero.

Interestingly, when the concentration of HF molecules increases, instead of forming AlF_3, the F atoms bind randomly to Al atoms. Similar to our T = 0 (Figure 1a–h) the AIMD simulations also clearly indicate that the formation of AlF_3 is not a spontaneous process. With increasing concentration of HF, the formation of AlF_3 and H_2 is observed (AlF_3 by dark orange and cyan colors, and H_2 by dark pink color). The number of H/F terminations also increases with concentration of HF, leading to large interlayer separation. To understand the effects of temperature, we performed AIMD simulations for 18% HF concentration at 500 K, and observed the dynamics for 10 ps. The higher temperature further increases the rate of reaction as can be observed by larger interlayer separation and lesser number of Al attached to $MXene_{up}$ in Figure S3. A previous study[44] also reported a faster conversion of MAX into MXene when the temperature was increased from 20 to 50 °C.

Electronic Structure and Charge Transfer. To understand the electronic origin of the exfoliation and functionalization processes, we analyzed the effects of step-by-step HF intercalation on the electronic structure of Ti_3AlC_2 (Figure 3a–h). First, we show the atom-projected density of states (PDOS) of MAX phase in Figure 3a. The strong overlap of Ti and C states, well below the Fermi energy, indicates the higher stability of Ti–C bonds.[45] The Ti1 states hybridize with the Al1 states; however, the finite density of states at the Fermi level renders the Al–MXene bond weaker and chemically more active than the Ti–C bond (Figure 3a). Relative to Ti (inside bulk type region) or Al (at edge), the large number of Ti1 (at edge) states at the Fermi level can be attributed to the edge effects (Figure S4).

Upon intercalation of first HF, the strong hybridization between the F (H) and the Ti1 (Ti2) states leads to robust binding between F1 (H) and Ti1 (Ti2) atoms. The Ti1 and Ti2 states, available at the Fermi level in MAX, shift to higher energy after the adsorption of H and F1, thus revealing the transfer of Ti electrons to F states. Relative to MAX, weaker overlap between Ti1 and Ti2 with Al1 states indicates weakening of Al1–Ti1 and Al1–Ti2 bond upon H/F termination (Figure 3b). Strong hybridization between F1 and F2 with Ti1 and Ti2 atoms, respectively, can be seen in Figure 3c. In three HF-intercalated MAX, F3 and H bonding states have substantial overlap with Al1 and Ti3 states, respectively (Figure 3d). It indicates strong binding between Al1 and F3 and H and Ti3. When a fourth HF intercalates, due to considerably large overlap between F4 and Ti1 states, these atoms bind strongly. The robust binding between the F1 and the F4 with Ti1 weakens the Al1–Ti1 (Figure 3e) bond. Weak binding between F4 and Ti2 can be inferred from the weak hybridization between F4 and Ti2 states. When a fifth HF intercalates, the F5 (H) states below the Fermi level overlap with Al1 (Ti3) states strongly, leading to the formation of strong Al1–F5 (H–Ti3) bonds (Figure 3f). Weak bonding between Al1–H and F3–H is evident from the weak overlap between the states of Al1 and F3 with H. In six HF-intercalated MAX, the strong bonding between Al1–F5 and Al1–F6 can be inferred from the large overlap between Al1–F5 and Al1–F6 bonding states (Figure 3g). Large overlap between the Al1 and F5 and F6 states below the Fermi level results in strong binding between Al1 and F5/F6. Strong hybridization of H states with Ti3 and Ti4 states essentially leads to the weakening of Al1 binding with both Ti3 and Ti4. Weak hybridization among Al1, F3, and F4 states is clearly shown in Figure 3h. While the states of F1 and F2 hybridize strongly with states of Ti1 and Ti2, respectively, weak hybridization between states of F4 (F3) and

DOI: 10.1021/acsami.6b08413
ACS Appl. Mater. Interfaces 2016, 8, 24256–24264

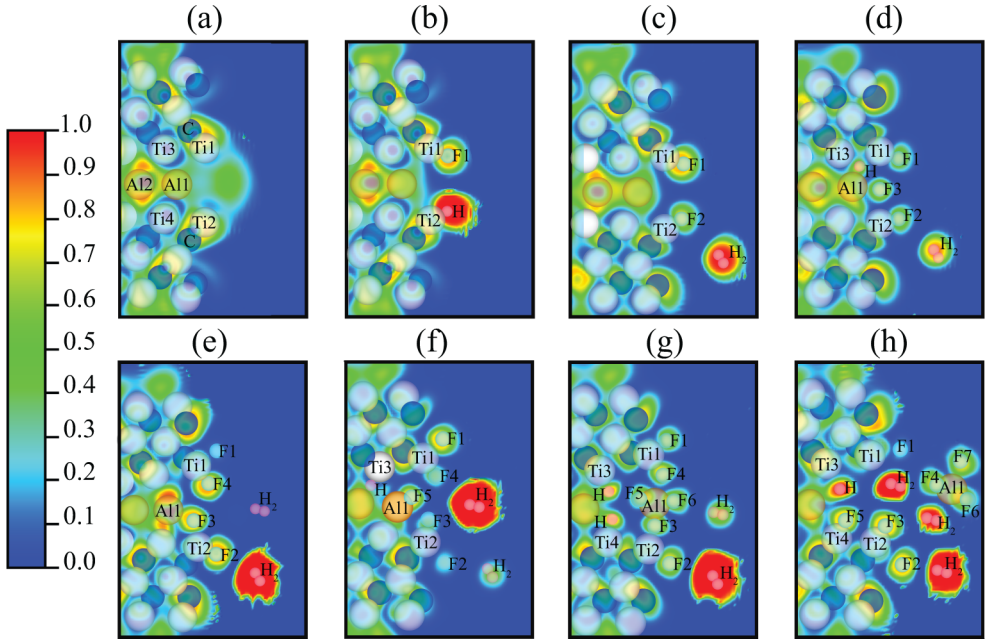

Figure 4. Electron localization function plots for (a) pristine and (b–h) 1–7 HF-intercalated Ti_3AlC_2.

Ti1 (Ti2) leads to dissociation of these bonds. Upon intercalation of a seventh HF, strong hybridization of Al1 with F4, F6, and F7 states results in the formation of AlF_3 molecules (Figure 3h). Large splitting between bonding and antibonding Al1, F4, F6, and F7 states further stabilizes the AlF_3 molecules. Strong hybridization between F5 (H) states and Ti3 (Ti4) show the formation of these bonds (Figure 3h), leading to functionalization of MXene.

The above analysis clearly show that due to strong binding between F/H and Ti atoms the HF intercalation into MAX will always facilitate isolation of functionalized MXene. Further, to elucidate the nature of bonds formed during the intercalation process between F/H and Al/Ti, we show the electron localization function for MAX and HF-intercalated MAX in Figure 4a–h. First, introduced by A. D. Becke and K. E. Edgecombe,[46] the electron localization function (ELF) simply relates the localization of an electron with the probability density of finding a second same spin electron near the reference point. The maximum value attended by the ELF = 1 corresponds to the perfect localization with respect to the uniform electron gas. ELF = 1/2 corresponds to electron-gas-like pair probability, and ELF = 0 indicates completely delocalized electrons. Strongly localized electron density (ELF ≈ 0.8–0.9) between Ti and C clearly indicates strong covalent bonding between Ti and C, whereas relatively weak bonding between Al and Ti is evident from the moderate ELF value (~0.4–0.6). For edge Ti–Al bonds, the electron density is localized on Al atoms, thus giving ionic character to the bond (Figure4a). The spilled over charge density in the region between the MXene layers essentially leads to dissociation of HF followed by their adsorption over the edge Ti1 and Ti2 atoms. Formation of strong covalent–ionic bonds between F/H and Ti are indicated by the presence of electron density between these atoms, which is mostly localized (ELF ≈ 0.8–1.0) on F/H atoms (Figure 4b–h). Formation of H_2 molecules is shown by the strong localization of a pair of electron (Figure 4c–h). Termination of Ti by F/H results in severe weakening of Ti–Al bonds (ELF ≈ 0.1) as shown in Figure 4b–h. Intercalation of a seventh HF results in the formation of AlF_3 as shown in Figure 4h. The ELF analysis also reveals the strong covalent–ionic binding between the Ti and the F atoms, which results in weakening of Al–Ti bonds and eventually leads to removal of Al from the MAX. This strong binding between Ti–F/H promotes the isolation of F-functionalized MXene.

Thermodynamics of the Exfoliation and Functionalization of MXene. The above analyses show that isolation of F-functionalized MXene is highly favorable. However, the random and nonuniform distribution of functional groups found in experimental studies reveals the difficulties associated with the stoichiometry ($Ti_3C_2F_x$, x = 0–2) control over the exfoliated functionalized MXene. To capture the complexity of the exfoliation and functionalization process, we study the thermodynamics of the reaction between MAX and HF.

First, we estimate the temperature range favorable for removal of Al. As shown above (Figure 1), removal of Al from MAX proceeds via formation of AlF_3. Therefore, the chemical potential of Al in AlF_3 should be lower than that in Ti_3AlC_2, i.e., $\mu_{Al}(AlF_3) < \mu_{Al}(Ti_3AlC_2)$. The chemical potential of Al in bulk AlF_3 and bulk Ti_3AlC_2 satisfies the following relations

$$E_{AlF_3} = \mu_{Al} + 3\mu_F \quad (1)$$

$$E_{Ti_3AlC_2} = 3\mu_{Ti} + \mu_{Al} + 2\mu_C \quad (2)$$

Using eqs 1 and 2, the above inequality relation can be expressed as $E_{AlF_3} - 3\mu_F < E_{Ti_3AlC_2} - 3\mu_{Ti} - 2\mu_C$. The chemical potential of Ti and C is referenced to the total energy of bulk Ti and graphite. The HF solution is considered as a reservoir for F atoms, whose total energy E_{HF} is given by $E_{HF} = \mu_F + \mu_H$. As the chemical potential of species in solution crucially depends upon the experimental growth conditions and can be controlled externally, it should be treated as variable. Under F-rich conditions, the μ_F can be referenced to the $\frac{1}{2}\mu_F[F_2]$. Under F-poor condition, the HF dissociates into H_2 and F_2 gas; therefore, $\mu_F = E_{HF} - \frac{1}{2}\mu_H[H_2]$. Here, the chemical potential of H is referenced to the total energy of H_2 molecules. We find

DOI: 10.1021/acsami.6b08413
ACS Appl. Mater. Interfaces 2016, 8, 24256–24264

that the formation of AlF_3 is preferred over Ti_3AlC_2 at any feasible chemical potential of F, except at very high temperature (Figure S5 in the Supporting Information).

After confirming the preference for the formation of AlF_3 relative to Ti_3AlC_2, next we study the thermodynamics of the functionalization process. We calculated the changes in Gibbs free energy (G) upon the HF intercalation, i.e., ΔG defined as $\Delta G = \Sigma\Delta G^{products} - \Sigma\Delta G^{reactants}$ (as discussed in Supporting Information). It allows comparison of the stabilities of reactants and various plausible products. The more negative ΔG the larger the thermodynamic driving force for the reaction. For evaluation of G of the model MAX and functionalized MXene, we considered a $2 \times 2 \times 1$ supercell. Following are the possible reactions considered in this study

$$Ti_{12}Al_4C_8 \rightarrow Ti_{12}C_8 + 4Al \quad (3)$$

$$Ti_{12}Al_4C_8 + 4HF \rightarrow Ti_{12}C_8F_4 + 4Al + 2H_2 \quad (4)$$

$$Ti_{12}Al_4C_8 + 12HF \rightarrow Ti_{12}C_8 + 4AlF_3 + 6H_2 \quad (5)$$

$$Ti_{12}Al_4C_8 + 14HF \rightarrow Ti_{12}C_8F_2 + 4AlF_3 + 7H_2 \quad (6)$$

$$Ti_{12}Al_4C_8 + 16HF \rightarrow Ti_{12}C_8F_4 + 4AlF_3 + 8H_2 \quad (7)$$

Here we utilized the fact that the chemical potentials of species are equal to the partial molar Gibbs free energy of that species.[47] For reaction 3, ΔG is positive, indicating that isolation of MXene in the absence of HF is not possible. The negative ΔG values are obtained for reactions 5−7, indicating that the formation AlF_3 is thermodynamically favorable, which is in agreement with the experiments.[1] In the entire range of μ_F, the ΔG for fully fluorinated and pristine MXene have the lowest and highest values, respectively (Figure S6 in the Supporting Information). Therefore, the formation of fully F-functionalized MXene is thermodynamically most favorable. However, negative ΔG for the formation of partially functionalized or pristine MXene indicates that these possibilities cannot be ruled out completely. Although, ΔG is negative for reaction 4, it is much higher than that of any other possible reactions. It shows that the formation of Al bulk, as one of the products, is thermodynamically not favorable.

As found above, the presence of water supports the exfoliation process by terminating the MXene layers by an OH functional group. Therefore, it is important to elucidate the effect of H_2O on the exfoliation and relative stabilities of fully, partially, or mixed functionalized MXene using thermodynamical considerations. Due to the presence of water both OH and O terminations are predicted and studied extensively.[8,48−50] At ambient conditions, however, only F and OH terminations are reported by experimental studies.[48] The O termination is a derived process and occurs at very high temperature, ∼1500 K.[48] The H from the OH group forms H_2 molecules and escapes, leaving the O-terminated MXene layers behind. Moreover, a high energy barrier of 1.6 eV[48] needs to be crossed for the transformation of OH into O, rendering the process unlikely at ambient conditions. Therefore, in the present work, we will consider only F and OH terminations. The following reactions are considered

$$Ti_{12}Al_4C_8 + 14HF + 2H_2O \rightarrow Ti_{12}C_8F_2(OH)_2 + 4AlF_3 + 8H_2 \quad (8)$$

$$Ti_{12}Al_4C_8 + 12HF + 2H_2O \rightarrow Ti_{12}C_8(OH)_2 + 4AlF_3 + 7H_2 \quad (9)$$

$$Ti_{12}Al_4C_8 + 13HF + H_2O \rightarrow Ti_{12}C_8F(OH) + 4AlF_3 + 7H_2 \quad (10)$$

$$Ti_{12}Al_4C_8 + 15HF + H_2O \rightarrow Ti_{12}C_8F_3(OH) + 4AlF_3 + 8H_2 \quad (11)$$

$$Ti_{12}Al_4C_8 + 12HF + 4H_2O \rightarrow Ti_{12}C_8(OH)_4 + 4AlF_3 + 8H_2 \quad (12)$$

The OH can come from H_2O, and the chemical potential of OH and H are related through the relation $E_{H_2O} = \mu_H + \mu_{OH}$. Since now the H atoms can come from any of the two sources, i.e, HF or H_2O, three chemical potentials, μ_H, μ_F, and μ_{OH}, are no longer independent of each other. Under these conditions, instead of setting H_2 gas as reference for H, it is useful to consider variable μ_H bounded by maxima and minima in H_2O and HF solution. In the H-rich limit, the $\mu_H = \frac{1}{2}\mu_H[H_2]$. In the H-poor limit, both HF and H_2O can dissociate; therefore, a lower bound can be calculated by setting the $\mu_F/\mu_{OH} = 0$ using either of the following relations

$$\mu_H = \Delta H_f^{H_2O} - \mu_{OH} \quad (13)$$

$$\mu_H = \Delta H_f^{HF} - \mu_F \quad (14)$$

Here, experimental values of $\Delta H_f^{H_2O}$ and ΔH_f^{HF} are taken.[51−53] The presence of water significantly modifies the experimentally accessible range of μ_H. Using eqs 13 and 14, the lowest bound for μ_H is calculated to be −5.90 and −6.25 eV, respectively. The common range for μ_H among eqs 13 and 14 is from −5.90 to −3.39 eV. The ΔG is calculated for eqs 5−12 across this shared range of μ_H and shown in Figure 5. It is evident that for any experimentally accessible μ_H there is a strong preference for the formation of fully F-functionalized MXene. Interestingly, the ΔG for mixed or partially functionalized and pristine MXene is also negative, thus indicating the finite probability of finding all of these in experiments. Most importantly, the ΔG for mixed

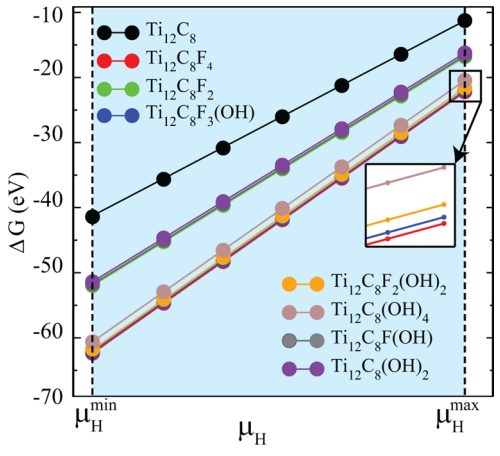

Figure 5. Change in the Gibbs free energy of reaction (ΔG) as a function of hydrogen chemical potential for different possible reaction paths.

DOI: 10.1021/acsami.6b08413
ACS Appl. Mater. Interfaces 2016, 8, 24256−24264

functionalized MXene is only slightly more in energy than that for fully F-functionalized MXene. Therefore, the mixed functionalization of MXene is also highly probable. The ΔG increases with the concentration of −OH present on the MXene, indicating a strong thermodynamic preference for the F terminations compared to OH terminations. Recently, an NMR study[15] on the surface structure of Ti_3C_2 MXene also revealed significantly fewer OH (and O) than F terminations. Due to the higher electronegativity of F compared to OH[54] ions, the charge transfer between the Ti atoms of MXene and terminating group will be large for F, which renders F−Ti bonds stronger than the Ti−OH bonds. The F terminations provide higher stability to the structure, and hence, fully F terminations are more favorable than mixed F/OH-terminated MXene.

From the above discussion it is clear that all the reactions, eqs 5−12 are thermodynamically possible and can occur with different probability, which depends upon the respective ΔG. The lower the ΔG, the higher the preference for that reaction. The reaction between MAX and HF will start with the formation of fully F-functionalized MXene. As the reaction progresses, the concentration of F goes down and the mixed functionalized MXene formation will start. With decreasing concentration of F, the various MXene shown in Figure 5 will form. In agreement with the experiments, thermodynamic analyses clearly indicate the random and nonuniform functionalization of MXene during the exfoliation process.

Degradation of MXene. Experimental studies on MXenes mainly focused on the exfoliation process; rarely any attention is devoted to understand the other possible reactions occurring concurrent to the exfoliation of MXene. Degradation of MXene at longer time scale also needs immediate attention. Therefore, we extended the thermodynamics analysis to the following possible reactions of formation of $TiF_4/TiF_3/TiO_2$ and graphite

$$Ti_3AlC_2 + 6H_2O + 3HF \rightarrow 3TiO_2 + AlF_3 + 2C + \frac{15}{2}H_2 \quad (15)$$

$$Ti_3AlC_2 + 12HF \rightarrow 3TiF_3 + AlF_3 + 2C + 6H_2 \quad (16)$$

$$Ti_3AlC_2 + 15HF \rightarrow 3TiF_4 + AlF_3 + 2C + 6H_2 \quad (17)$$

Although a high concentration of HF or H_2O is required, negative and large ΔG values for the reactions 15−17 (Figure S7) indicate the finite probability of the formation of $TiF_3/TiF_4/TiO_2$ and graphite. Indeed, disorders/defects in MXene have been reported in a recent study when the high concentration of HF was used to exfoliate MXene. An experimental study[55] has recently reported the formation of TiO_2 during the conversion of MAX into MXene. Therefore, the transformation of MAX into MXene is usually carried out in low-concentration HF solution.[56] The strong preference for the formation of TiO_2 (Figure S7) indicates that in the moist environment there will be a good chance of MXene to be converted to TiO_2. These challenges associated with the exfoliation and long-term stability of MXene must be kept in mind while fabricating the MXene-based devices for practical applications.

CONCLUSION

In conclusion, using first-principles calculations we studied the detailed mechanism of exfoliation and functionalization processes of MXene using HF intercalation via the edges of MAX. By considering step-by-step intercalation of HF molecules into MAX, we show that the termination of MXene by F/H atoms of HF molecule leads to weakening of Al−Ti bonds. The opening of the interlayer gap, due to this weakening, permits further intercalation of HF molecules and results in formation of AlF_3. H_2O supports the reaction by terminating the MXene by OH. PDOS and ELF analyses also indicate that functionalization of MXene is essentially due to the formation of strong Ti−F bonds. The negative and very close Gibbs free energies for the formation of fully F- and mixed F/OH-functionalized MXene support the random functionalization of MXene. Although high in energy, ΔG is negative for partially functionalized or pristine MXene, indicating the formation of nonuniformly functionalized MXene. The exfoliation of MXene from MAX using HF is a fairly general route for the synthesis of MXene. Therefore, results presented in this study reveal the microscopic details of the exfoliation process of MXene in general and provide explanation for the thermodynamically driven challenges associated with control over the functionalization of MXenes. The thermodynamics analyses of other possible reactions indicate that the higher concentration of HF/H_2O will cause degradation of the MXene structure; therefore, these reactions need to be carried out under milder conditions. These issues necessarily call for the development of alternative routes for exfoliation of MXene, circumventing the difficulties related to the controlled functionalization of MXene.

ASSOCIATED CONTENT

Supporting Information

This material is available free of charge via the Internet at http://pubs.acs.org/. The Supporting Information is available free of charge on the ACS Publications website at DOI: 10.1021/acsami.6b08413.

Model structure of MAX, intercalation of H_2O molecule via edge of MAX, AIMD snapshots revealing temperature effect on exfoliation, PDOS of Ti atom at edge relative to those inside the bulk, variation of μ_{Al} in MAX and AlF_3 with respect to μ_F, ΔG as a function μ_F for formation of MXene with varying degrees of functionalization and ΔG as a function of μ_H for the formation of $TiF_4/TiF_3/TiO_2$; short discussion regarding the calculation of formation energy and ΔG (PDF)

AUTHOR INFORMATION

Corresponding Author

*E-mail: abhishek@mrc.iisc.ernet.in.

Author Contributions

‡P.S. and A.M. contributed equally.

Notes

The authors declare no competing financial interest.

ACKNOWLEDGMENTS

We acknowledge financial support of the Korea Institute of Science and Technology (Grant No. 2E26130). We thank the Materials Research Centre and Supercomputer Education and Research Centre of Indian Institute of Science and the IMR supercomputers facility at Tohoku University, Japan, for providing computing facilities for completion of this work. A.K.S. and A.M. acknowledge support from DST Nanomission.

DOI: 10.1021/acsami.6b08413
ACS Appl. Mater. Interfaces 2016, 8, 24256−24264

REFERENCES

(1) Naguib, M.; Kurtoglu, M.; Presser, V.; Lu, J.; Niu, J.; Heon, M.; Hultman, L.; Gogotsi, Y.; Barsoum, M. W. Two-Dimensional Nanocrystals Produced by Exfoliation of Ti_3AlC_2. *Adv. Mater.* **2011**, *23*, 4248−4253.

(2) Shein, I. R.; Ivanovskii, A. L. Graphene-Like Nanocarbides and Nanonitrides of *d* Metals (MXenes): Synthesis, Properties and Simulation. *Micro Nano Lett.* **2013**, *8*, 59−62.

(3) Tang, Q.; Zhou, Z.; Shen, P. Are MXenes Promising Anode Materials for Li Ion Batteries? Computational Studies on Electronic Properties and Li Storage Capability of Ti_3C_2 and $Ti_3C_2X_2$ (X = F, OH) Monolayer. *J. Am. Chem. Soc.* **2012**, *134*, 16909−16916.

(4) Naguib, M.; Halim, J.; Lu, J.; Cook, K. M.; Hultman, L.; Gogotsi, Y.; Barsoum, M. W. New Two-Dimensional Niobium and Vanadium Carbides as Promising Materials for Li-Ion Batteries. *J. Am. Chem. Soc.* **2013**, *135*, 15966−15969.

(5) Er, D.; Li, J.; Naguib, M.; Gogotsi, Y.; Shenoy, V. B. Ti_3C_2 MXene as a High Capacity Electrode Material for Metal (Li, Na, K, Ca) Ion Batteries. *ACS Appl. Mater. Interfaces* **2014**, *6*, 11173−11179.

(6) Ling, Z.; Ren, C. E.; Zhao, M.-Q.; Yang, J.; Giammarco, J. M.; Qiu, J.; Barsoum, M. W.; Gogotsi, Y. Flexible and Conductive MXene Films and Nanocomposites with High Capacitance. *Proc. Natl. Acad. Sci. U. S. A.* **2014**, *111*, 16676−16681.

(7) Lukatskaya, M. R.; Mashtalir, O.; Ren, C. E.; Dall'Agnese, Y.; Rozier, P.; Taberna, P. L.; Naguib, M.; Simon, P.; Barsoum, M. W.; Gogotsi, Y. Cation Intercalation and High Volumetric Capacitance of Two-Dimensional Titanium Carbide. *Science* **2013**, *341*, 1502−1505.

(8) Xie, Y.; Dall'Agnese, Y.; Naguib, M.; Gogotsi, Y.; Barsoum, M. W.; Zhuang, H. L.; Kent, P. R. C. Prediction and Characterization of MXene Nanosheet Anodes for Non-Lithium-Ion Batteries. *ACS Nano* **2014**, *8*, 9606−9615.

(9) Hu, Q.; Sun, D.; Wu, Q.; Wang, H.; Wang, L.; Liu, B.; Zhou, A.; He, J. MXene: A New Family of Promising Hydrogen Storage Medium. *J. Phys. Chem. A* **2013**, *117*, 14253−14260.

(10) Hu, Q.; Wang, H.; Wu, Q.; Ye, X.; Zhou, A.; Sun, D.; Wang, L.; Liu, B.; He, J. Two-dimensional Sc_2C: A Reversible and High-Capacity Hydrogen Storage Material Predicted by First-Principles Calculations. *Int. J. Hydrogen Energy* **2014**, *39*, 10606−10612.

(11) Rasool, K.; Helal, M.; Ali, A.; Ren, C. E.; Gogotsi, Y.; Mahmoud, K. A. Antibacterial Activity of $Ti_3C_2T_x$ MXene. *ACS Nano* **2016**, *10*, 3674−3684.

(12) Halim, J.; Lukatskaya, M. R.; Cook, K. M.; Lu, J. C.; Smith, C. R.; Naslund, L. A.; May, S. J.; Hultman, L.; Gogotsi, Y.; Eklund, P.; Barsoum, M. W. Transparent Conductive Two-Dimensional Titanium Carbide Epitaxial Thin Films. *Chem. Mater.* **2014**, *26*, 2374.

(13) Mauchamp, V.; Bugnet, M.; Bellido, E. P.; Botton, G. A.; Moreau, D.; Magne, P.; Naguib, M.; Cabio'h, T.; Barsoum, M. W. Enhanced and Tunable Surface Plasmons in Two-Dimensional Ti_3C_2 Stacks: Electronic Structure Versus Boundary Effects. *Phys. Rev. B: Condens. Matter Mater. Phys.* **2014**, *89*, 235428.

(14) Hantanasirisakul, K.; Zhao, M.-Q.; Urbankowski, P.; Halim, J.; Anasori, B.; Kota, S.; Ren, C. E.; Barsoum, M. W.; Gogotsi, Y. Fabrication of $Ti_3C_2T_x$ MXene Transparent Thin Films with Tunable Optoelectronic Properties. *Adv. Electron. Mater.* **2016**, *2*, 1600050.

(15) Hope, M. A.; Forse, A. C.; Griffith, K. J.; Lukatskaya, M. R.; Ghidiu, M.; Gogotsi, Y.; Grey, C. P. NMR Reveals the Surface Functionalisation of Ti_3C_2 MXene. *Phys. Chem. Chem. Phys.* **2016**, *18*, 5099.

(16) Berdiyorov, G. R.; Madjet, M. E.; Mahmoud, K. A. Ionic Sieving Through $Ti_3C_2(OH)_2$ MXene: First-Principles Calculations. *Appl. Phys. Lett.* **2016**, *108*, 113110.

(17) Khazaei, M.; Arai, M.; Sasaki, T.; Ranjbar, A.; Liang, Y.; Yunoki, S. OH-Terminated Two-Dimensional Transition Metal Carbides and Nitrides as Ultralow Work Function Materials. *Phys. Rev. B: Condens. Matter Mater. Phys.* **2015**, *92*, 075411.

(18) Tang, Q.; Zhou, Z.; Shen, P. Are MXenes Promising Anode Materials for Li Ion Batteries? Computational Studies on Electronic Properties and Li Storage Capability of Ti_3C_2 and $Ti_3C_2X_2$ (X = F, OH) Monolayer. *J. Am. Chem. Soc.* **2012**, *134*, 16909−16916.

(19) Segal, M. Selling Graphene by The Ton. *Nat. Nanotechnol.* **2009**, *4*, 612−614.

(20) Stankovich, S.; Dikin, D. A.; Piner, R. D.; Kohlhaas, K. A.; Kleinhammes, A.; Jia, Y.; Wu, Y.; Nguyen, S. T.; Ruoff, R. S. Synthesis of Graphene-Based Nanosheets via Chemical Reduction of Exfoliated Graphite Oxide. *Carbon* **2007**, *45*, 1558−1565.

(21) Eda, G.; Fanchini, G.; Chhowalla, M. Large-Area Ultrathin Films of Reduced Graphene Oxide as a Transparent and Flexible Electronic Material. *Nat. Nanotechnol.* **2008**, *3*, 270−274.

(22) Li, X.; Zhang, G.; Bai, X.; Sun, X.; Wang, X.; Wang, E.; Dai, H. Highly Conducting Graphene Sheets and Langmuir-Blodgett Films. *Nat. Nanotechnol.* **2008**, *3*, 538−542.

(23) Ang, P. K.; Wang, S.; Bao, Q.; Thong, J. T.; Loh, K. P. High-Throughput Synthesis of Graphene by Intercalation-Exfoliation of Graphite Oxide and Study of Ionic Screening in Graphene Transistor. *ACS Nano* **2009**, *3*, 3587−3594.

(24) Ambrosi, A.; Sofer, Z.; Pumera, M. Lithium Intercalation Compound Dramatically Influences the Electrochemical Properties of Exfoliated MoS_2. *Small* **2015**, *11*, 605−612.

(25) Sresht, V.; Pádua, A. A.; Blankschtein, D. Liquid-Phase Exfoliation of Phosphorene: Design Rules from Molecular Dynamics Simulations. *ACS Nano* **2015**, *9*, 8255−8268.

(26) Enyashin, A. N.; Ivanovskii, A. L. Structural and Electronic Properties and Stability of MXenes Ti_2C and Ti_3C_2 Functionalized by Methoxy Groups. *J. Phys. Chem. C* **2013**, *117*, 13637−13643.

(27) Khazaei, M.; Arai, M.; Sasaki, T.; Chung, C.-Y.; Venkataramanan, N. S.; Estili, M.; Sakka, Y.; Kawazoe, Y. Novel Electronic and Magnetic Properties of Two-Dimensional Transition Metal Carbides and Nitrides. *Adv. Funct. Mater.* **2013**, *23*, 2185−2192.

(28) Kurtoglu, M.; Naguib, M.; Gogotsi, Y.; Barsoum, M. W. First Principles Study of Two-Dimensional Early Transition Metal Carbides. *MRS Commun.* **2012**, *2*, 133−137.

(29) Xie, Y.; Kent, P. R. C. Hybrid Density Functional Study of Structural and Electronic Properties of Functionalized $Ti_{n+1}X_n$ (*X* = C, N) Monolayers. *Phys. Rev. B: Condens. Matter Mater. Phys.* **2013**, *87*, 235441.

(30) Blöchl, P. E. Projector Augmented-Wave Method. *Phys. Rev. B: Condens. Matter Mater. Phys.* **1994**, *50*, 17953−17979.

(31) Kresse, G.; Joubert, D. From Ultrasoft Pseudopotentials to the Projector Augmented-Wave Method. *Phys. Rev. B: Condens. Matter Mater. Phys.* **1999**, *59*, 1758−1775.

(32) Kresse, G.; Furthmüller, J. Efficiency of Ab-Initio Total Energy Calculations for Metals and Semiconductors Using a Plane-Wave Basis Set. *Comput. Mater. Sci.* **1996**, *6*, 15−50.

(33) Perdew, J. P.; Burke, K.; Ernzerhof, M. Generalized Gradient Approximation Made Simple [Phys. Rev. Lett. 77, 3865 (1996)]. *Phys. Rev. Lett.* **1997**, *78*, 1396−1396.

(34) Monkhorst, H. J.; Pack, J. D. Special Points for Brillouin-Zone Integrations. *Phys. Rev. B* **1976**, *13*, 5188−5192.

(35) Nosé, S. A Unified Formulation of the Constant Temperature Molecular Dynamics Methods. *J. Chem. Phys.* **1984**, *81*, 511−519.

(36) Hoover, W. G. Canonical Dynamics: Equilibrium Phase-Space Distributions. *Phys. Rev. A: At., Mol., Opt. Phys.* **1985**, *31*, 1695−1697.

(37) Shuichi, N. Constant Temperature Molecular Dynamics Methods. *Prog. Theor. Phys. Supp.* **1991**, *103*, 1−46.

(38) Park, J. S.; Yu, L.; Lee, C. S.; Shin, K.; Han, J. H. Liquid-Phase Exfoliation of Expanded Graphites into Graphene Nanoplatelets Using Amphiphilic Organic Molecules. *J. Colloid Interface Sci.* **2014**, *417*, 379−384.

(39) Xu, J.; Dang, D. K.; Tran, V. T.; Liu, X.; Chung, J. S.; Hur, S. H.; Choi, W. M.; Kim, E. J.; Kohl, P. A. Liquid-Phase Exfoliation of Graphene in Organic Solvents with Addition of Naphthalene. *J. Colloid Interface Sci.* **2014**, *418*, 37−42.

(40) Yoon, G.; Seo, D.-H.; Ku, K.; Kim, J.; Jeon, S.; Kang, K. Factors Affecting the Exfoliation of Graphite Intercalation Compounds for Graphene Synthesis. *Chem. Mater.* **2015**, *27*, 2067−2073.

(41) Mishra, A.; Srivastava, P.; Mizuseki, H.; Lee, K.-R.; Singh, A. K. Isolation of Pristine MXene from Nb_4AlC_3 MAX Phase: A First-Principles Study. *Phys. Chem. Chem. Phys.* **2016**, *18*, 11073−11080.

DOI: 10.1021/acsami.6b08413
ACS Appl. Mater. Interfaces 2016, 8, 24256−24264

(42) Ling, C.; Shi, L.; Ouyang, Y.; Chen, Q.; Wang, J. Transition Metal-Promoted V_2CO_2 (MXenes): A New and Highly Active Catalyst for Hydrogen Evolution Reaction. *Adv. Sci.* **2016**, 1600180.
(43) Mukhopadhyay, S.; Bailey, C.; Wander, A.; Searle, B.; Muryn, C.; Schroeder, S.; Lindsay, R.; Weiher, N.; Harrison, N. Stability of the AlF_3 (0 0 $\bar{1}$ 2) Surface in H_2O and HF Environments: An Investigation Using Hybrid Density Functional Theory and Atomistic Thermodynamics. *Surf. Sci.* **2007**, *601*, 4433−4437.
(44) Mashtalir, O.; Naguib, M.; Dyatkin, B.; Gogotsi, Y.; Barsoum, M. W. Kinetics of aluminum extraction from Ti_3AlC_2 in hydrofluoric acid. *Mater. Chem. Phys.* **2013**, *139*, 147−152.
(45) Naguib, M.; Mochalin, V. N.; Barsoum, M. W.; Gogotsi, Y. 25th Anniversary Article: MXenes: A New Family of Two-Dimensional Materials. *Adv. Mater.* **2014**, *26*, 992−1005.
(46) Becke, A. D.; Edgecombe, K. E. A Simple Measure of Electron Localization in Atomic and Molecular Systems. *J. Chem. Phys.* **1990**, *92*, 5397−5403.
(47) Binninger, T.; Mohamed, R.; Waltar, K.; Fabbri, E.; Levecque, P.; Kötz, R.; Schmidt, T. J. Thermodynamic Explanation of the Universal Correlation between Oxygen Evolution Activity and Corrosion of Oxide Catalysts. *Sci. Rep.* **2015**, *5*, 12167.
(48) Xie, Y.; Naguib, M.; Mochalin, V. N.; Barsoum, M. W.; Gogotsi, Y.; Yu, X.; Nam, K.-W.; Yang, X.-Q.; Kolesnikov, A. I.; Kent, P. R. C. Role of Surface Structure on Li-Ion Energy Storage Capacity of Two-Dimensional Transition-Metal Carbides. *J. Am. Chem. Soc.* **2014**, *136*, 6385−6394.
(49) Bai, Y.; Zhou, K.; Srikanth, N.; Pang, J. H.; He, X.; Wang, R. Dependence of Elastic and Optical Properties on Surface Terminated Groups in Two-Dimensional MXene Monolayers: A First-Principles Study. *RSC Adv.* **2016**, *6*, 35731−35739.
(50) Yu, Y.-X. Prediction of Mobility, Enhanced Storage Capacity, and Volume Change during Sodiation on Interlayer-Expanded Functionalized Ti_3C_2 MXene Anode Materials for Sodium-Ion Batteries. *J. Phys. Chem. C* **2016**, *120*, 5288−5296.
(51) Vedeneyev, V.; Gurvich, L. V.; Kondrat 'Yev, V.; Technica, S. *Bond Energies, Ionization Potentials and Electron Affinities*; St. Martin's Press: New York, 1966.
(52) Herzberg, G.; Monfils, A. The Dissociation Energies of the H_2, HD, and D_2 Molecules. *J. Mol. Spectrosc.* **1961**, *5*, 482−498.
(53) Johns, J. W. C.; Barrow, R. F. The Ultra-Violet Spectra of HF and DF. *Proc. R. Soc. London, Ser. A* **1959**, *251*, 504−518.
(54) Lindquist, B. A.; Woon, D. E.; Dunning, T. H. Effects of Ligand Electronegativity on Recoupled Pair Bonds with Application to Sulfurane Precursors. *J. Phys. Chem. A* **2014**, *118*, 5709−5719.
(55) Ying, Y.; Liu, Y.; Wang, X.; Mao, Y.; Cao, W.; Hu, P.; Peng, X. Two-Dimensional Titanium Carbide for Efficiently Reductive Removal of Highly Toxic Chromium(VI) from Water. *ACS Appl. Mater. Interfaces* **2015**, *7*, 1795−1803.
(56) Wang, H.-W.; Naguib, M.; Page, K.; Wesolowski, D. J.; Gogotsi, Y. Resolving the Structure of $Ti_3C_2T_x$ MXenes through Multilevel Structural Modeling of the Atomic Pair Distribution Function. *Chem. Mater.* **2016**, *28*, 349−359.

DOI: 10.1021/acsami.6b08413
ACS Appl. Mater. Interfaces 2016, 8, 24256−24264